

Quantitative Assessment of Atypical Birefringence Images Using Scanning Laser Polarimetry With Variable Corneal Compensation

HARMOHINA BAGGA, MD, DAVID S. GREENFIELD, MD, AND WILLIAM J. FEUER, MS

- **PURPOSE:** To define the clinical characteristics of atypical birefringence images and to describe a quantitative method for their identification.
- **DESIGN:** Prospective, comparative, clinical observational study.
- **METHODS:** Normal and glaucomatous eyes underwent complete examination, standard automated perimetry, scanning laser polarimetry with variable corneal compensation (GDx-VCC), and optical coherence tomography (OCT) of the macula, peripapillary retinal nerve fiber layer (RNFL), and optic disk. Eyes were classified into two groups: normal birefringence pattern (NBP) and atypical birefringence pattern (ABP). Clinical, functional, and structural characteristics were assessed separately. A multiple logistic regression model was used to predict eyes with ABP on the basis of a quantitative scan score generated by a support vector machine (SVM) with GDx-VCC.
- **RESULTS:** Sixty-five eyes of 65 patients were enrolled. ABP images were observed in 5 of 20 (25%) normal eyes and 23 of 45 (51%) glaucomatous eyes. Compared with eyes with NBP, glaucomatous eyes with ABP demonstrated significantly lower SVM scores ($P < .0001$, 0.008 , 0.03 , and 0.03 , respectively) and greater temporal, mean, inferior, and nasal RNFL thickness using GDx-VCC; and a weaker correlation with OCT generated RNFL thickness ($R^2 = .75$ vs $.27$). ABP images were significantly correlated with older age ($R^2 = .16$, $P = .001$). The SVM score was the only significant

($P < .0001$) predictor of ABP images and provided high discriminating power between eyes with NBP and ABP (area under the receiver operator characteristic curve = 0.98).

- **CONCLUSIONS:** ABP images exist in a subset of normal and glaucomatous eyes, are associated with older patient age, and produce an artifactual increase in RNFL thickness using GDx-VCC. The SVM score is highly predictive of ABP images. (Am J Ophthalmol 2005;139:437–446. © 2005 by Elsevier Inc. All rights reserved.)

THE BASIC PATHOLOGIC CHANGE IN GLAUCOMA IS loss of retinal ganglion cells and their axons resulting in retinal nerve fiber layer (RNFL) atrophy and the optic nerve head changes pathognomic of glaucoma. Scanning laser polarimetry is one of the imaging modalities available for quantitative assessment of RNFL. Linearly polarized light traversing the RNFL is elliptically polarized, and the amount of linear retardation of light at each corresponding retinal location is proportional to the RNFL thickness.

To neutralize the confounding influence of corneal birefringence on RNFL thickness, the latest commercial polarimeter has an integrated variable corneal compensator, which determines and neutralizes eye-specific corneal polarization axis and magnitude using the concept of the macula as an intraocular polarimeter.^{1–4} Several studies have shown that SLP with variable corneal compensation (GDx-VCC) significantly improves the structure-function relationship,^{5–7} agreement with other imaging technologies,^{6,8} and discriminating power for glaucoma detection^{4,9,10} compared with scanning laser polarimetry with fixed corneal compensation.

Atypical patterns of peripapillary birefringence have been observed in a subset of normal and glaucomatous eyes. Such images deviate from the normal pattern of birefringence generally characterized by the presence of high peripapillary retardation superiorly and inferiorly that

Accepted for publication Oct 7, 2004.

From the Department of Ophthalmology, University of Miami School of Medicine, Bascom Palmer Eye Institute, Miami, Florida.

Supported in part by the Maltz Family Endowment for Glaucoma Research, Cleveland, Ohio; the New York Community Trust, New York, New York; a grant from Mr. Barney Donnelley, Palm Beach, Florida; and National Institute of Health grant R01-EY08684, Bethesda, Maryland.

Presented in part at the annual meeting of the International Society for Imaging in the Eye (ISIE), Fort Lauderdale, Florida, April 24, 2004.

Inquiries to David S. Greenfield, MD, Bascom Palmer Eye Institute, 7108 Fairway Drive, Suite 340, Palm Beach Gardens, Florida 33418; fax: (561) 515-1588; e-mail: dgreenfield@med.miami.edu

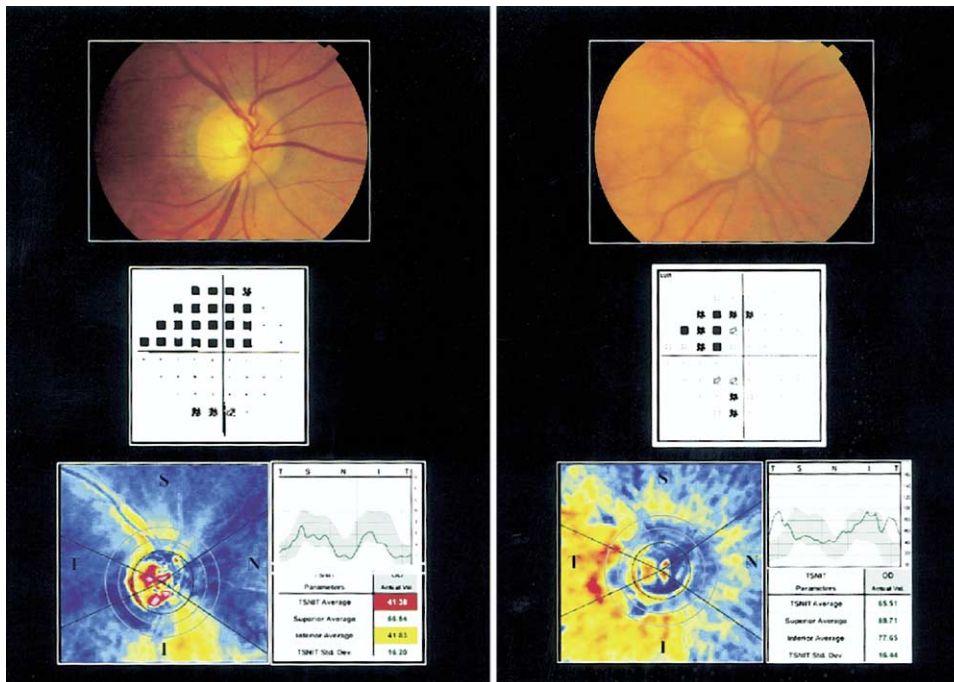


FIGURE 1. Normal birefringence pattern compared with atypical birefringence pattern. Optic nerve photo (top row), standard automated visual field (middle row), and scanning laser polarimetry with variable corneal compensation (GDx-VCC) image (bottom row) in two glaucomatous eyes with normal birefringence pattern (left panel) and atypical birefringence pattern (right panel) characterized by alternating rings of low and high peripapillary retardation. Note the normal retardation parameters in the ABP image compared with the NBP image that demonstrates a significant reduction in the temporal, superior, nasal, inferior, temporal (TSNIT) average ($P < .5\%$) and inferior average retinal nerve fiber layer thickness ($P < 1\%$).

corresponds histologically to the distribution of the superior and inferior arcuate nerve fiber bundles. We hypothesized that an atypical birefringence artifact can confound the detection and quantification of glaucomatous damage. The purpose of this investigation was to define the clinical characteristics of atypical birefringence images and to describe a quantitative method for their identification.

PATIENTS AND METHODS

NORMAL AND GLAUCOMATOUS EYES MEETING ELIGIBILITY criteria were enrolled in this prospective study. Normal subjects represented volunteers from the Bascom Palmer Eye Institute and private patients. Informed consent was obtained from all subjects by a consent form approved by the Institutional Review Board for Human Research of the University of Miami School of Medicine, and all procedures adhered to the tenets of the Declaration of Helsinki. All patients underwent complete ophthalmic examination including slit-lamp biomicroscopy, gonioscopy, pachymetry, Goldmann applanation tonometry, dilated stereoscopic examination of the optic disk and fundus, and standard automated perimetry (SAP). Optical coherence tomography (OCT) and GDx-VCC imaging were performed by one experienced operator (H.B.) within 6 months of the clinical examination. One eye per subject

was enrolled. If both eyes met the eligibility criteria, one eye was randomly selected.

Normal subjects had no history of ocular disease. All had intraocular pressure (IOP) less than or equal to 21 mm Hg by Goldmann applanation tonometry, normal optic disk appearance based on clinical stereoscopic examination and review of stereodisk photography, and normal perimetry. Absence of glaucomatous optic neuropathy was defined as vertical cup-disk asymmetry less than 0.2, cup-to-disk ratio less than 0.6, and intact neuroretinal rim without peripapillary hemorrhages, notches, localized pallor, or RNFL defect. Normal visual field indices were defined as a mean defect and corrected standard deviation within 95% confidence limits and a glaucoma hemifield test result within normal limits.

Glaucomatous optic neuropathy was defined as either cup-disk asymmetry between fellow eyes of greater than 0.2, rim thinning, notching, excavation, or RNFL defect. SAP was performed with the Humphrey Field Analyzer (Carl-Zeiss Meditec, Dublin, California) using a Swedish Interactive Testing algorithm standard strategy, program 24-2. Patients with visual field abnormalities had at least one confirmatory visual field examination. Visual field abnormality was defined as GHT outside normal limits and pattern standard deviation of probability $< 5\%$. Eyes with visual acuity less than 20/40, peripapillary atrophy extending to 1.7 mm from disk center, retinal disease, or unreliable SAP (greater than 25% fixation losses, false-positive,

TABLE 1. Clinical and Structural Characteristics of Normal Subjects (n = 20) With Normal Birefringence (NBP) and Atypical Birefringence Patterns (ABP)

	NBP (n = 15)	ABP (n = 5)	P Value
Mean age (years) ± SD	54 ± 17	69 ± 14	.11 [†]
Sex			
Male	7	1	.30*
Female	8	4	
Race			
White	13	4	.15*
Hispanic	2	0	
Black	0	1	
Mean IOP (mm Hg) ± SD	13.0 ± 2.0	16.0 ± 4.0	.20 [†]
Mean refractive error (D) ± SD	0.4 ± 2.5	-1.0 ± 3.7	.38 [†]
Mean central corneal thickness (μm) ± SD	559.3 ± 9.6	562.4 ± 16.6	.87 [†]
Mean corneal polarization axis (degrees) ± SD	19.8 ± 17.0	20.3 ± 11.0	.95 [†]
Mean corneal polarization magnitude (nm) ± SD	35.0 ± 13.8	47.6 ± 9.1	.07 [†]
Mean visual field mean deviation (dB) ± SD	-0.3 ± 1.3	0.2 ± 0.6	.40 [†]
Mean OCT RNFL thickness (μm) ± SD	91.8 ± 7.2	92.7 ± 9.8	.84 [†]
GDx-VCC parameters			
Mean SVM score	94.5 ± 6.8	48.4 ± 31.7	<.0001 [†]
Mean temporal average (μm) ± SD	25.3 ± 6.8	39.3 ± 6.7	.0008 [†]
Mean RNFL thickness (μm) ± SD	53.8 ± 2.8	59.1 ± 3.0	.002 [†]
Mean inferior average (μm) ± SD	61.2 ± 3.8	67.0 ± 3.4	.007 [†]
Mean TSNIT SD (μm) ± SD	21.8 ± 5.2	18.0 ± 3.5	.14 [†]
Mean nasal average (μm) ± SD	42.2 ± 9.1	45.4 ± 6.7	.50 [†]
Mean superior average (μm) ± SD	65.2 ± 7.1	67.1 ± 6.6	.61 [†]
Mean NFI	18.5 ± 6.6	19.4 ± 4.6	.77 [†]
Mean residual corneal birefringence ± SD	5.4 ± 2.5	6.0 ± 1.6	.62 [†]
<p>GDx-VCC = scanning laser polarimetry with variable corneal compensation; IOP = intraocular pressure; NBP = normal birefringence pattern; NFI = nerve fiber indicator; OCT = optical coherence tomography; RNFL = retinal nerve fiber layer; SD = standard deviation; SVM = support vector machine; TSNIT = temporal, superior, nasal, inferior, temporal.</p> <p>*Chi-square test. [†]Student t test.</p>			

and false-negative rates) were excluded from this investigation.

OCT imaging (Stratus OCT, Carl-Zeiss Meditech) of the peripapillary RNFL, optic nerve head (ONH) and macula were performed in all patients within 6 months of clinical examination using version 3.0 software. Topographic measurements of the ONH using OCT are generated by identifying the edge of the optic nerve head as the termination of the retinal pigment epithelium/choriocapillaris layer and defining a parallel line 150 μm anteriorly. ONH images were obtained using six radial scans in a spokelike pattern, each 4 mm long, centered on the optic disk. Macular thickness measurements were generated using six radial lines, each 6 mm long, centered on the fovea, to generate a macular map of 6 mm diameter. Data from the central 0.5 mm of the map were excluded because the foveola is devoid of ganglion cells. Images with poor centration, focus, or with a signal-to-noise ratio below 33 dB were excluded (3.0 Stratus OCT User's Manual, pp. 6-3).

GDx-VCC imaging (GDx-VCC, Laser Diagnostic Technology, San Diego, California, USA) was performed using a circular scan (3.2 mm diameter) centered on the optic disk as described previously.^{6,11,12} Images were excluded that were obtained during eye movement, as well as unfocused, poorly centered images or images with a quality score grade less than 8. Based on the pattern of the retardation map, images were classified into two groups: normal birefringence pattern (NBP) and atypical birefringence pattern (ABP). NBP images were defined as retardation maps with highest retardation superiorly and inferiorly and low retardation nasally and temporally. ABP images were defined as retardation maps with alternating peripapillary circumferential bands of low and high retardation, variable areas of high retardation arranged in a spokelike peripapillary pattern, or splotchy areas of high retardation nasally and temporally. A quantitative scan score (0–100 with lower scores associated with greater image atypia) based on a support vector machine (SVM) analysis was generated automatically for each image with

TABLE 2. Clinical and Structural Characteristics of Glaucomatous Subjects (n = 45) With Normal Birefringence (NBP) and Atypical Birefringence Patterns (ABP)

	NBP (n = 22)	ABP (n = 23)	P Value
Mean age (years) ± SD	65 ± 13	74 ± 7	.007 [†]
Sex			
Male	7	7	.92*
Female	15	16	
Race			
White	17	23	.02*
Hispanic	3	0	
Black	2	0	
Mean refractive error (D) ± SD	0.03 ± 2.5	-1.0 ± 2.3	.20 [†]
Mean IOP (mm Hg) ± SD	15.0 ± 4.0	13.0 ± 4.0	.10 [†]
Mean central corneal thickness (μm) ± SD	542.7 ± 30.0	539.3 ± 35.4	.73 [†]
Mean corneal polarization axis (degrees) ± SD	12.0 ± 10.4	17.0 ± 11.4	.14 [†]
Mean corneal polarization magnitude (nm) ± SD	39.6 ± 16.8	36.0 ± 14.4	.45 [†]
Mean visual field mean deviation (dB) ± SD	-9.3 ± 11.4	-8.0 ± 8.1	.66 [†]
Mean OCT RNFL thickness (μm) ± SD	67.0 ± 22.8	65.9 ± 18.6	.86 [†]
GDx-VCC parameters			
Mean SVM score	93.7 ± 6.2	35.7 ± 32.0	<.0001 [†]
Mean temporal average (μm) ± SD	30.0 ± 8.5	45.0 ± 13.4	<.0001 [†]
Mean RNFL thickness (μm) ± SD	43.2 ± 10.8	52.2 ± 10.9	.008 [†]
Mean inferior average (μm) ± SD	48.0 ± 14.3	58.1 ± 15.5	.03 [†]
Mean nasal average (μm) ± SD	35.0 ± 9.5	41.3 ± 10.0	.03 [†]
Mean superior average (μm) ± SD	49.6 ± 16.2	55.8 ± 11.8	.15 [†]
Mean TSNIT SD (μm) ± SD	15.1 ± 7.6	13.5 ± 4.8	.40 [†]
Mean NFI	56.3 ± 32.4	42.3 ± 24.9	.11 [†]
Mean residual corneal birefringence ± SD	5.2 ± 2.9	5.0 ± 2.5	.78 [†]

D = diopters; GDx-VCC = scanning laser polarimetry with variable corneal compensation; IOP = intraocular pressure; NBP = normal birefringence pattern; NFI = nerve fiber indicator; OCT = optical coherence tomography; RNFL = retinal nerve fiber layer; SD = standard deviation; SVM = support vector machine; TSNIT = temporal, superior, nasal, inferior, temporal; VCC = variable corneal compensation.

*Chi-square test.

[†]Student t test.

TABLE 3. Correlation Between GDx-VCC Average RNFL Thickness, Visual Field Mean Deviation (MD), and Structural Assessment Using OCT in Eyes (n = 65) With Normal Birefringence (NBP) and Atypical Birefringence Patterns (ABP)

	NBP (n = 39)		ABP (n = 26)		NBP vs ABP (n = 65)
	R ²	P Value	R ²	P Value	P Value
Visual field MD (dB) ± SD	.71	<.0001	.42	.0002	.09
OCT RNFL thickness (μm) ± SD	.75	<.0001	.29	.005	.01
Rim area (mm ²) ± SD	.76	<.0001	.27	.02	.004
Rim volume (mm ³) ± SD	.48	.0007	.28	.01	.30
Vertical cup-to-disc ratio	.41	.003	.19	.05	.26
Mean macular thickness (μm) ± SD	.33	.0002	.21	.02	.57

ABP = atypical birefringence pattern; GDx-VCC = scanning laser polarimetry with variable corneal compensation; NBP = normal birefringence pattern; OCT = optical coherence tomography; RNFL = retinal nerve fiber layer.

GDx-VCC. The SVM score is based on the slope, standard deviation, and average magnitude of the RNFL thickness measurements from the edge of the optic nerve head extending outward to 20 degrees. The slope, standard

deviation, and average magnitude are calculated separately for each quadrant (superior, inferior, temporal, and nasal) and along a wedge in each quadrant. SVM scores were analyzed separately in normal and glaucomatous eyes using

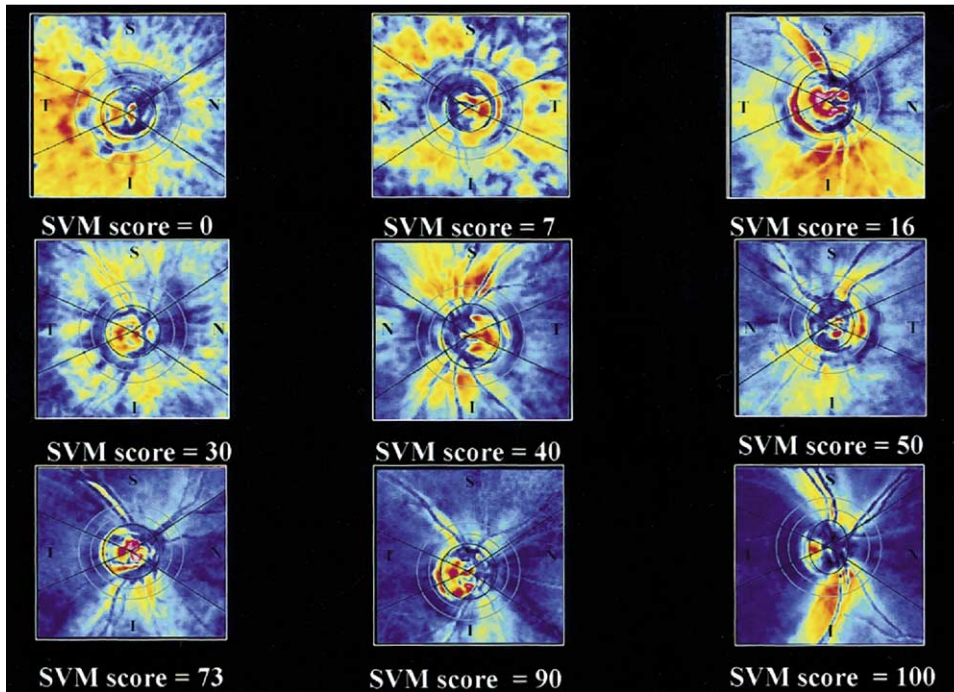


FIGURE 2. Scanning laser polarimetry with variable corneal compensation (GDx-VCC) and support vector machine score. GDx-VCC retinal nerve fiber layer thickness retardation images and the respective support vector machine (SVM) scores are illustrated in nine subjects. Note that the overall posterior segment retardation and magnitude of ABP image atypia increases with decreased SVM score.

multiple logistic regression analysis to provide an objective means of predicting the probability of ABP images.

Statistical analysis was performed using JMP (SAS Institute) and SPSS software (Chicago, IL). Bivariate Pearson correlations were calculated and multiple linear regression models were constructed to determine the influence of SVM score on RNFL assessments using GDx-VCC. A logistic regression model was constructed to determine whether SVM score was a significant predictor of ABP images as well as to determine the probability of ABP images separately in normal and glaucomatous eyes at a given SVM score. Receiver operator characteristic (ROC) curves and the area under the receiver operating characteristic (AUROC) curves were quantified for SVM using the method described by Hanley and associates.¹³ A *P* value less than or equal to .05 was considered statistically significant.

RESULTS

SIXTY-FIVE EYES OF SIXTY-FIVE PATIENTS (45 GLAUCOMA, 20 normal) were enrolled (mean age 66 ± 14 years, range 28–85). Average visual field mean deviation (MD) in glaucomatous eyes was -8.6 ± 9.8 dB (range 1.9–32.8). ABP images were observed in 5 of 20 (25%) normal eyes, and 23 of 45 (51%) glaucomatous eyes. Figure 1 illustrates the characteristic retardance map in two glaucomatous

eyes with an NBP image (left panel) and ABP image (right panel) characterized by alternating rings of low and high peripapillary retardation. Note the normal retardation parameters in the ABP image compared with the NBP image that demonstrates a significant reduction in the temporal, superior, nasal, inferior, temporal (TSNIT) average ($P < .5\%$) and inferior average RNFL thickness ($P < 1\%$).

Tables 1 and 2 illustrate the clinical and structural characteristics of the study population in normal and glaucomatous eyes, respectively. Compared with eyes with NBP, glaucomatous eyes with ABP demonstrated a significantly ($P < .0001$, <0.0001 , 0.008 , 0.03 , and 0.03 , respectively) lower SVM score and greater temporal, mean, inferior, and nasal RNFL thickness using GDx-VCC. As demonstrated in Table 2, although the severity of visual field and OCT-generated RNFL atrophy were similar in eyes with NBP and ABP, eyes with ABP had significantly greater measured RNFL thickness using GDx-VCC.

Table 3 demonstrates the correlation between GDx-VCC mean RNFL thickness visual field mean deviation, and structural assessments using OCT in eyes with NBP and ABP. Compared with eyes with NBP, eyes with ABP demonstrated a weaker correlation with visual field MD ($R^2 = .71$ vs $.42$, $P = .09$), and OCT generated RNFL thickness ($R^2 = .75$ vs $.29$, $P = .01$), macular thickness ($R^2 = .33$ vs $.21$, $P = .57$), vertical CDR ($R^2 = .41$ vs $.19$,

TABLE 4. Correlation Between the SVM Score, Clinical Characteristics, and Structural Assessments (n = 65)

	SVM Score	
	R ²	P Value
Mean age (years) ± SD	.16	.001
Mean refractive error (D) ± SD	.03	.20
Mean IOP (mm Hg) ± SD	<.0001	.98
Mean central corneal thickness (μm) ± SD	.01	.50
Mean visual field MD (dB) ± SD	.001	.78
Mean OCT RNFL thickness (μm) ± SD	.06	.06
GDx-VCC parameters		
Mean temporal average (μm) ± SD	.65	<.0001
Mean inferior average (μm) ± SD	.13	.003
Mean RNFL thickness (μm) ± SD	.16	.001
Mean TSNIT SD (μm) ± SD	.05	.06
Mean nasal average (μm) ± SD	.05	.07
Mean superior average (μm) ± SD	.01	.33
Mean NFI ± SD	.01	.55
Mean residual birefringence (μm) ± SD	.0003	.90
Mean corneal birefringence axis	.005	.58
Mean corneal retardance (μm) ± SD	.01	.37

ABP = atypical birefringence pattern; CCT = central corneal thickness; GDx-VCC = scanning laser polarimetry with variable corneal compensation; IOP = intraocular pressure; MD = mean deviation; NFI = nerve fiber indicator; OCT = optical coherence tomography; SVM = support vector machine; TSNIT = temporal, superior, nasal, inferior, temporal.

$P = .26$), rim area ($R^2 = .76$ vs $.27$, $P = .004$), and rim volume ($R^2 = .48$ vs $.28$, $P = .3$). These respective correlations were weakened by assessing the entire group ($n = 65$) without separately extracting the eyes with ABP for visual field MD ($R^2 = .51$ vs $.71$), OCT generated RNFL thickness ($R^2 = .41$ vs $.75$), macular thickness ($R^2 = .15$ vs $.33$), vertical CDR ($R^2 = .18$ vs $.41$), rim area ($R^2 = .36$ vs $.76$), and rim volume ($R^2 = .28$ vs $.48$). The discriminating power of mean RNFL thickness using GDx-VCC was greater ($P = .38$) in eyes with NBP (AUROC = $.86$) compared with eyes with ABP (AUROC = $.77$) but was not statistically significant.

The mean SVM score of the study population was 69.9 ± 35.1 (range 0–100). Mean SVM score was significantly ($P < .0001$) higher in normal and glaucomatous eyes with NBP images (94.5 ± 6.8 , 93.7 ± 6.4) compared with ABP images (48.4 ± 31.7 , 35.7 ± 32.0). Figure 2 illustrates the GDx-VCC RNFL retardation images and the respective SVM scores in nine subjects. Note that the overall posterior segment retardation and magnitude of ABP image atypia increases with decreased SVM score.

Table 4 demonstrates the correlation between the SVM score, clinical characteristics, and structural assessments in normal and glaucomatous eyes ($n = 65$). Among the study population ($n = 65$), the SVM score negatively correlated with older age ($R^2 = .16$, $P = .001$) but did not correlate

($P > .05$) with refractive error, sex, corneal birefringence axis or magnitude, central corneal thickness, visual field MD, or OCT RNFL thickness. The SVM score strongly correlated ($R^2 = .65$, $P < .0001$) with temporal RNFL thickness using GDx-VCC. Furthermore, the SVM score demonstrated a significant correlation with mean RNFL thickness ($R^2 = .16$, $P = .001$) and inferior average ($R^2 = .13$, $P = .003$) RNFL thickness using GDx-VCC. Multiple linear regression models were constructed to predict the influence of the SVM score on GDx-VCC-generated RNFL thickness measurements. The SVM score was found to significantly ($P < .0001$) influence the temporal RNFL thickness so that a decrease in the SVM score by 1 U produced an increased temporal RNFL thickness by 2.2 μm. Figure 3 illustrates a scatterplot of temporal RNFL thickness values against the SVM score ($R^2 = .65$, $P < .0001$). Eyes with NBP tended to have higher SVM scores and lower temporal RNFL thickness values; eyes with ABP demonstrated relatively lower SVM scores and increased temporal RNFL thickness values.

Figure 4 illustrates the distributions of SVM scores for NBP and ABP images in normal and glaucomatous eyes as box and whisker plots. Horizontal lines indicate medians; boxes indicate the 25th and 75th percentiles; whiskers provide an estimate of the range. Note that there is little overlap between the subjective grading of birefringence patterns and the SVM scores, suggesting that the SVM scores provided excellent discrimination between atypical and normal birefringence patterns based on the subjective grading.

Using a multiple logistic regression model, the SVM score was the only significant ($P < .0001$) predictor of atypical birefringence. No relationship between the SVM score and presence or absence of glaucomatous damage was observed ($P = .77$), suggesting that at a given SVM score, the probability of an image with ABP is similar in normal and glaucomatous eyes. Figure 5 illustrates the predicted probability of an ABP image in normal and glaucomatous eyes given the SVM score. Eyes with an SVM score of ≤ 60 had a 100% probability of an ABP image in this cohort. Figure 6 illustrates the ROC curve for the SVM score and demonstrates a high discriminating power for separating eyes with NBP and ABP (AUROC = 0.98 , sensitivity 93%, specificity 92% at SVM score cutoff of 82.5).

DISCUSSION

GLAUCOMA IS A MULTIFACTORIAL OPTIC NEUROPATHY known to cause progressive loss of retinal ganglion cells and their axons leading to a reduction in the thickness of the RNFL. Imaging technologies such as scanning laser polarimetry and OCT represent useful methods for objective detection and quantification of glaucomatous RNFL atrophy. Both technologies have been demonstrated to

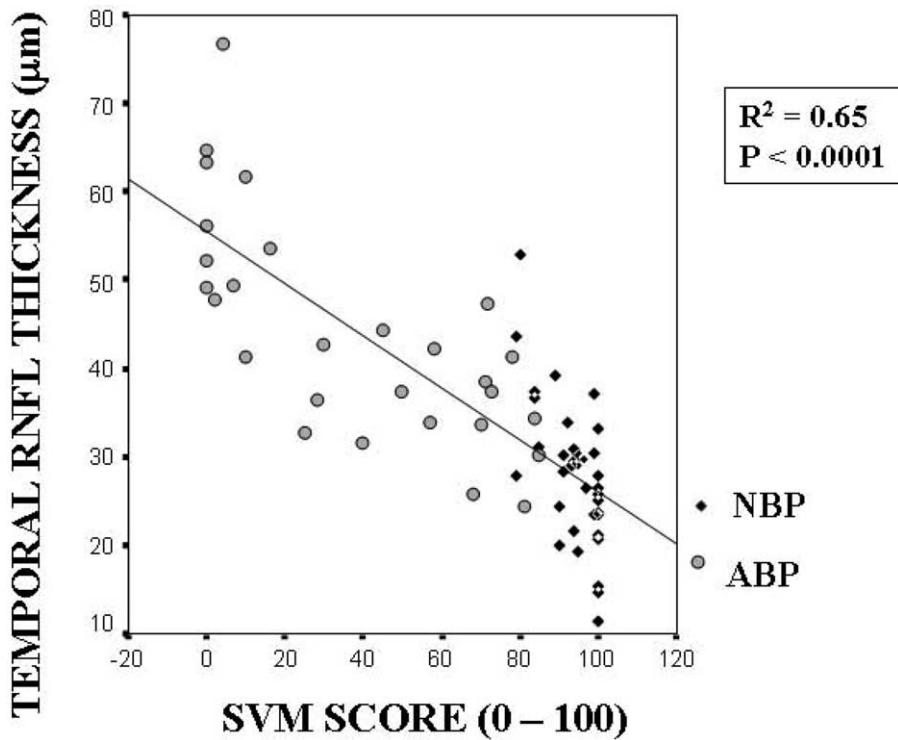


FIGURE 3. Temporal retinal nerve fiber layer thickness (RNFL) compared with support vector machine (SVM) score. Scatterplot of temporal RNFL thickness is illustrated against the SVM score ($R^2 = .65$, $P < .0001$). Eyes with normal birefringence pattern (NBP) tended to have higher SVM scores and lower temporal RNFL thickness values; eyes with atypical birefringence pattern (ABP) demonstrated relatively lower SVM scores and increased temporal RNFL thickness values.

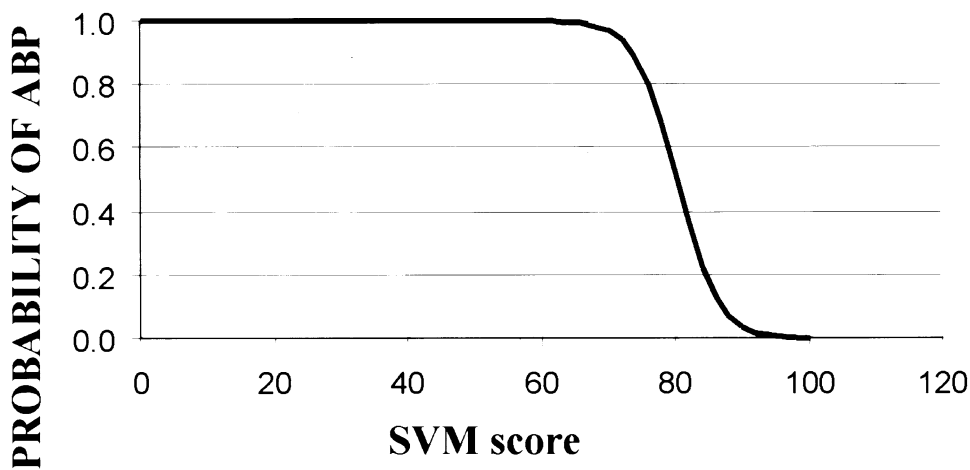


FIGURE 4. Distribution of support vector machine score. Distribution of support vector machine (SVM) scores for normal birefringence pattern (NBP) and atypical birefringence pattern (ABP) images in normal and glaucomatous eyes are illustrated as box and whisker plots. Horizontal lines indicate medians; boxes indicate the 25th and 75th percentiles; whiskers provide an estimate of the range. Note that there is little overlap between the subjective grading of birefringence patterns and the SVM scores, suggesting that the SVM scores provided excellent discrimination between atypical and normal birefringence patterns based on the subjective grading.

have high levels of reproducibility,¹⁴⁻¹⁹ incorporate age-matched normative data, and allow noninvasive assessment of the peripapillary RNFL²⁰⁻²⁴ through an undilated pupil.

GDx-VCC represents the latest commercial polarimeter and provides neutralization of eye-specific corneal birefringence axis and magnitude resulting in enhanced diagnostic accuracy.^{1,4-7,9,10,25} This study reveals that atypical images

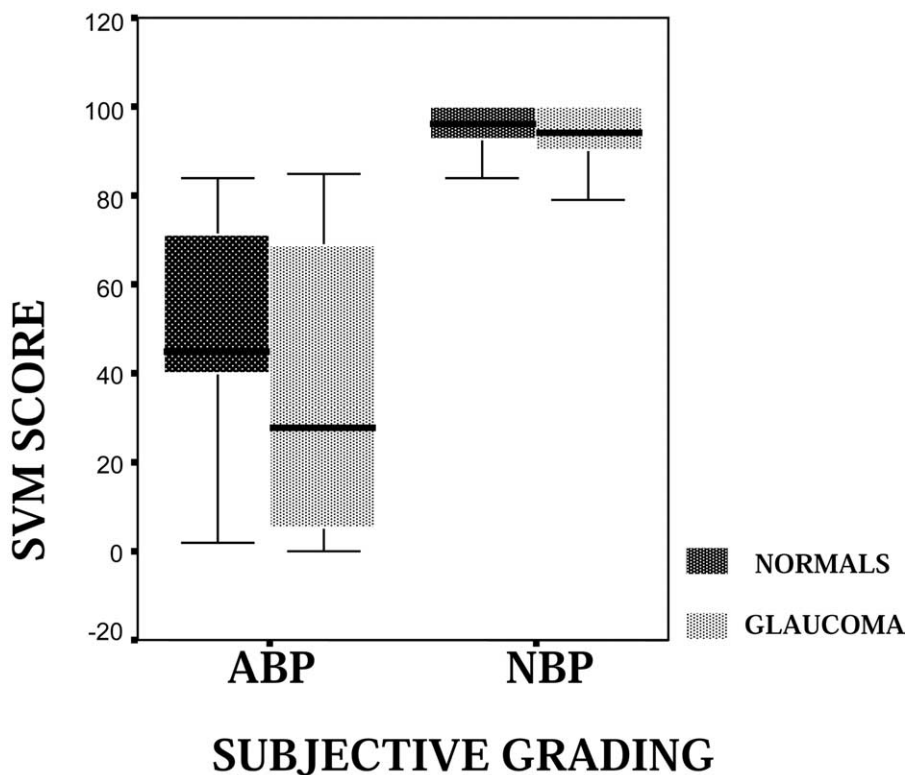


FIGURE 5. Probability of atypical birefringence pattern (ABP) image. Predicted probability of an atypical birefringence pattern given the support vector machine (SVM) score is illustrated in normal and glaucomatous eyes using multiple logistic regression analysis.

exist in a subset of normal and glaucomatous eyes. Because our study concerns nonconsecutive pilot data, the exact prevalence remains to be established in larger, consecutive, prospective series. It has been estimated that the overall prevalence of such images is approximately 10% (personal communication, Michael J. Sinai, Laser Diagnostic Technology, San Diego, California).

The pathophysiology of ABP images is unknown. It has been hypothesized that such images occur in the presence of low signal-to-noise ratio resulting from loss or diminution of reflectivity from the retinal pigment epithelium. The low signal-to-noise ratio produces an increased gain to augment the polarization signal, which paradoxically increases noise from deeper retinal structures such as the sclera. Although there has been speculation that such images are associated with high myopia, we found no significant relationship with refractive error, although eyes with ABP tended to be slightly more myopic. There was a significant association between ABP and increased age, which may reflect diminution of the retinal pigment epithelium with age. We also found a significantly higher prevalence of ABP images in Caucasian eyes with glaucoma, although the precise relationship between race and ABP is limited by our sample size.

Our data demonstrate that eyes with ABP have an increase in the apparent RNFL thickness using GDx-VCC.

Although glaucomatous eyes with ABP images had significantly greater mean, nasal, and inferior average RNFL thickness, the alteration in SNR was manifest most prominently in the temporal region of the peripapillary RNFL. Using multiple linear regression models, a decrease in SVM score by 1 U predicted overestimation of the temporal RNFL thickness by 2.2 μm , but prospective validation is warranted using an independent study population. The mechanism underlying this observation remains unclear but may in part be related to differences in the polarization characteristics or reflectivity of the temporal fundus. Further study is necessary to determine a causal relationship with axial length, ultrasound characteristics of posterior segment curvature, or differential fundus pigmentation.

Eyes with ABP had significantly weaker correlation with visual field MD and structural assessments generated with OCT (Table 3). Inclusion of such eyes will adversely affect the discriminating power of this technology. As expected, the discriminating power of GDx-VCC mean RNFL thickness was lower in eyes with ABP compared with eyes with NBP. Clinicians and investigators should be aware of this phenomenon and exhibit caution when interpreting the retardance parameters generated in such eyes. Software strategies to reduce and or correct ABP images would be

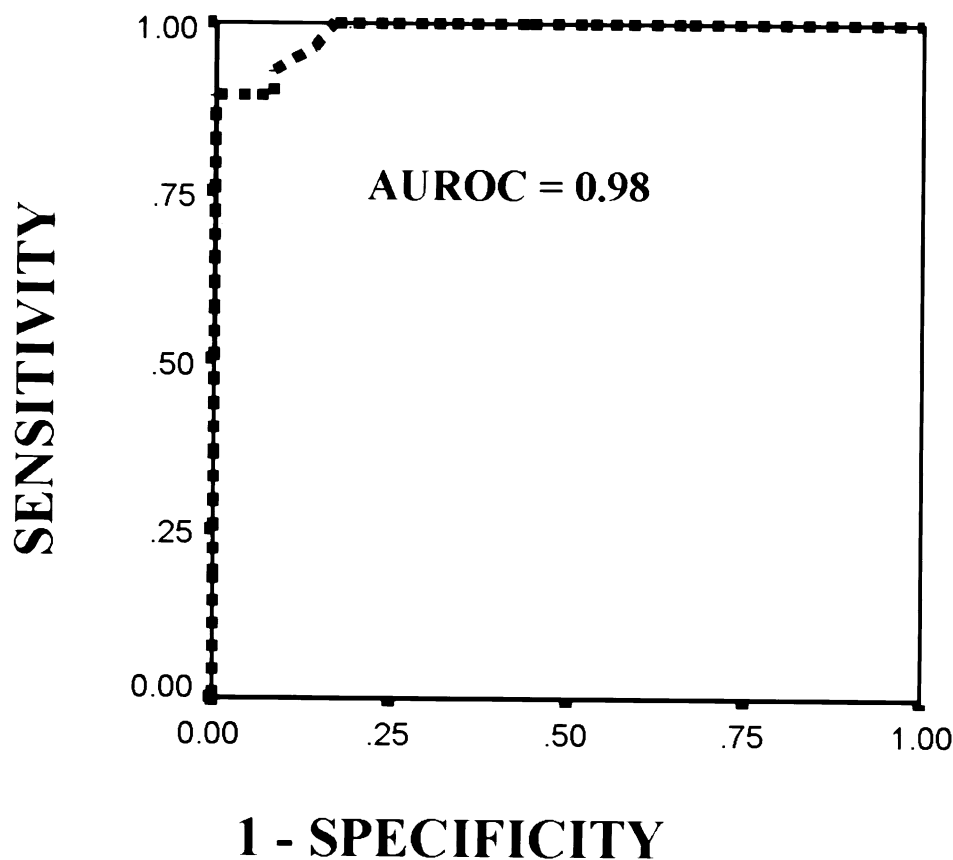


FIGURE 6. Discriminating power of support vector machine (SVM) score. Receiver operator characteristic (ROC) curve for SVM score in separating normal birefringence patterns from atypical birefringence (area under the receiver operating characteristic curve [AUROC]= 0.98, sensitivity 93%, specificity 92% with an SVM score cutoff of 82.5).

expected to further improve the diagnostic accuracy of this technology and are currently under investigation.

Our data demonstrate that the SVM score generated automatically by GDx-VCC software is a reliable predictor of ABP image artifact. As demonstrated in Figure 4, SVM scores ≤ 60 have a high probability of ABP. It should be noted, however, that the discriminating performance of the SVM score is fundamentally based on the subjective assessment of image quality and criteria for ABP images as defined in this investigation. The probability of atypical birefringence was similar in normal and glaucomatous eyes at any given SVM score. Furthermore, as illustrated in Figure 5, the SVM score had high diagnostic precision for discriminating eyes with NBP and ABP. These data suggest that the SVM score should be obtained in all subjects, and further studies involving GDx-VCC should consider exclusion of eyes with a score ≤ 60 .

In conclusion, ABP images exist in a subset of normal and glaucomatous eyes, are associated with older patient age, and produce an artifactual increase in RNFL thickness using GDx-VCC and a weak correlation with structural assessments obtained using OCT. The SVM score is highly predictive of ABP images and has high discriminating power between ABP and NBP images.

REFERENCES

1. Garway-Heath DF, Greaney MJ, Caprioli J. Correction for the erroneous compensation of anterior segment birefringence with the scanning laser polarimeter for glaucoma diagnosis. *Invest Ophthalmol Vis Sci* 2002;43:1465–1474.
2. Knighton RW, Huang X-R, Greenfield DS. Analytical model of scanning laser polarimetry for retinal nerve fiber layer assessment. *Invest Ophthalmol Vis Sci* 2002;43:383–392.
3. Zhou Q, Weinreb RN. Individualized compensation of anterior segment birefringence during scanning laser polarimetry. *Invest Ophthalmol Vis Sci* 2002;43:2221–2228.
4. Weinreb RN, Bowd C, Zangwill LM. Glaucoma detection using scanning laser polarimetry with variable corneal polarization compensation. *Arch Ophthalmol* 2003;120:218–224.
5. Schlottman PG, De Cilla S, Greenfield DS, Caprioli J, Garway-Heath DF. Relationship between visual field sensitivity and retinal nerve fiber layer thickness as measured by scanning laser polarimetry. *Invest Ophthalmol Vis Sci* 2004; 45:1823–1829.
6. Bagga H, Greenfield DS, Feuer W, Knighton RW. Scanning laser polarimetry with variable corneal compensation and optical coherence tomography in normal and glaucomatous eyes. *Am J Ophthalmol* 2003;135:521–529.
7. Bowd C, Zangwill LM, Weinreb RN. Association between scanning laser polarimetry measurements using variable cor-

- neal polarization compensation and visual field sensitivity in glaucomatous eyes. *Arch Ophthalmol* 2003;121:961–966.
8. Essock EA, Sinai MJ, Bowd C, Zangwill LM, Weinreb RN. Fourier analysis of optical coherence tomography and scanning laser polarimetry retinal nerve fiber layer measurements in the diagnosis of glaucoma. *Arch Ophthalmol* 2003;121:1238–1245.
 9. Greenfield DS, Knighton RW, Feuer W, Schiffman J, Zangwill L, Weinreb RN. Correction for corneal polarization axis improves the discriminating power of scanning laser polarimetry. *Am J Ophthalmol* 2002;134:27–33.
 10. Choplin NT, Zhou Q, Knighton RW. Effect of individualized compensation for anterior segment birefringence on retinal nerve fiber layer assessments as determined by scanning laser polarimetry. *Ophthalmology* 2003;110:719–725.
 11. Bagga H, Greenfield DS, Knighton RW. Scanning laser polarimetry with variable corneal compensation: identification and correction for corneal birefringence in eyes with macular pathology. *Invest Vis Sci Ophthalmol* 2003;44:1969–1976.
 12. Bagga H, Greenfield DS. Quantitative assessment of structural damage in eyes with localized visual field abnormalities. *Am J Ophthalmol* 2004;137:797–805.
 13. Hanley JA, McNeil BJ. A method of comparing the areas under receiver operating curves derived from the same cases. *Radiology* 1983;148:839–843.
 14. Schuman JS, Pedut-Kloizman T, Hertzmark E, et al. Reproducibility of nerve fiber layer thickness measurements using optical coherence tomography. *Ophthalmology* 1996;103:1889–1898.
 15. Blumenthal EZ, Williams JM, Weinreb RN, Girkin CA, Berry CC, Zangwill LM. Reproducibility of nerve fiber layer thickness measurements by use of optical coherence tomography. *Ophthalmology* 2000;107:2278–2282.
 16. Zangwill L, Berry CA, Garden VS, Weinreb RN. Reproducibility of retardation measurements with the Nerve Fiber Analyzer II. *J Glaucoma* 1997;6:384–389.
 17. Villain MA, Greenfield DS. Peripapillary nerve fiber layer thickness measurement reproducibility using optical coherence tomography. *Ophthalmic Surg Lasers Imaging* 2003;34:33–37.
 18. Rhee DJ, Greenfield DS, Chen PP, Schiffman J. Reproducibility of retinal nerve fiber layer thickness measurements using scanning laser polarimetry in pseudophakic eyes. *Ophthalmic Surg Lasers* 2002;33:117–122.
 19. Hoh ST, Ishikawa H, Greenfield DS, Liebmann JM, Chew SJ, Ritch R. Peripapillary nerve fiber layer thickness measurement reproducibility using scanning laser polarimetry. *J Glaucoma* 1998;7:12–15.
 20. Schuman JS, Hee MR, Puliafito CA, et al. Quantification of nerve fiber layer thickness in normal and glaucomatous eyes using optical coherence tomography. *Arch Ophthalmol* 1995;113:586–596.
 21. El Beltagi TA, Bowd C, Boden C, et al. Retinal nerve fiber layer thickness measured with optical coherence tomography is related to visual function in glaucomatous eyes. *Ophthalmology* 2003;110:2185–2191.
 22. Zangwill LM, Bowd C, Berry CC, et al. Discriminating between normal and glaucomatous eyes using the Heidelberg Retina Tomograph, GDx Nerve Fiber Analyzer, and Optical Coherence Tomograph. *Arch Ophthalmol* 2001;119:985–993.
 23. Zangwill LM, Williams J, Berry CC, Knauer S, Weinreb RN. A comparison of optical coherence tomography and retinal nerve fiber layer photography for detection of nerve fiber layer damage in glaucoma. *Ophthalmology* 2000;107:1309–1315.
 24. Nouri-Mahdavi K, Hoffman D, Tannenbaum D, Law SK, Caprioli J. Identifying early glaucoma with optical coherence tomography. *Am J Ophthalmol* 2004;137:228–235.
 25. Tannenbaum D, Hoffman D, Lemij HG, Garway-Heath DF, Greenfield DS, Caprioli J. Variable corneal compensation improves the discrimination between normal and glaucomatous eyes with the scanning laser polarimeter. *Ophthalmology* 2004;111:259–264.